Organic & Biomolecular Chemistry

PAPER

View Article Online
View Journal | View Issue

Cite this: *Org. Biomol. Chem.*, 2014, **12**, 6134

Balanced π–π interactions directing the self-assembly of indolocarbazole-based low molecular mass organogelators†

Peng Gong, Pengchong Xue, Chong Qian, Zhenqi Zhang and Ran Lu*

Received 29th April 2014,
Accepted 26th June 2014

DOI: 10.1039/c4ob00873a

www.rsc.org/obc

New indolocarbazole derivatives emitting strong blue light have been synthesized. It is found that the strong π–π interactions between indolocarbazoles **4–6** without long carbon chains lead to the formation of crystal or crystal-like aggregates. We have previously found that *tert*-butyl could tune the strength of π–π interactions between carbazole units and the organogels were obtained from *tert*-butyl substituted carbazoles directed by balanced π–π interactions. Herein, hexadecyl groups were introduced into N-positions of indolocarbazoles in order to reduce the strength of π–π interactions between indolocarbazoles, and compounds **7–9** were prepared. It is interesting that compounds **8** and **9** could form stable organogels in alcohols, acetone, DMSO, and so on, upon ultrasound stimulation. Combined with the results of electronic spectra, XRD patterns and the optimized molecular length based on the semiempirical (AM1) calculations, we suggested the molecular packing modes in gel states, in which the lamellar structures were involved. Although the fluorescence emission of indolocarbazoles **8** and **9** decreased during the gel formation to some extent, the obtained gel nanofibers still emitted strong blue light and the fluorescence emission of the film based on xerogel **9** decreased significantly upon exposure to gaseous TNT. It meant that the xerogels based on indolocarbazoles could be used as fluorescent sensors for detecting vapors of explosives.

Introduction

In recent years, the low molecular mass organogelators (LMOGs) bearing rigid π-conjugated units have drawn enormous attention because they can act as building blocks of functional supramolecular assemblies with well-ordered nanostructures, leading to special optoelectronic properties.[1–7] It is known that π-organogels have potential applications in the fields of optoelectronic devices, fluorescent sensors, light harvesting antennas, drug delivery, catalysis and template synthesis.[8–21] Although numerous conjugated skeletons, such as oligophenylenevinylene, perylene bisimide, β-diketone-boron difluoride, salene, benzoxazole, and cyanostilbene, have been introduced into π-gelators, the construction of new π-organogels with enhanced performance in optoelectronic devices is still challenging.[22–27] Notably, acenes, such as pentacene, which has been used as a benchmark in organic field-effect transistors (OFET) with a high mobility of 3 $cm^2 V^{-1} s^{-1}$, have received much attention due to their extended π-conjugated systems. However, they usually exhibit poor solubility in common organic solvents. The high crystallization directed by strong π–π interactions would decrease the stability of the concerned devices and limit their practical applications.[28,29] Till now, the gelation of low molecular mass organic π-gelators has been proven as an important strategy to arrange the chromophores into functional soft materials, in which the carrier mobility or the energy (or electron) transfer efficiency would be improved. Notably, as another kind of polycyclic aromatic systems, indolocarbazole derivatives have found applications in medicine and organic optoelectronic devices.[30–36] For example, Beng S. Ong *et al.* have synthesized 5,11-bis(4-octylphenyl)indolo[3,2-*b*]carbazole, which could be used as a p-channel semiconductor with good environmental stability for organic electronic applications owing to the relatively low-lying HOMO and large band gap. The mobility and the current on/off ratio of the indolo[3,2-*b*]carbazole-based OTFT (organic thin film transistor) were up to 0.12 $cm^2 V^{-1} s^{-1}$ and 10^7, respectively.[32] However, to the best of our knowledge, no report on the π-gelators based on indolocarbazole derivatives has been found. We anticipate that the unique properties of indolocarbazole derivatives will be acquired if ordered nano-

State Key Laboratory of Supramolecular Structure and Materials, College of Chemistry, Jilin University, Changchun 130012, P. R. China.
E-mail: luran@mail.jlu.edu.cn; Fax: +86-431-88499179

†Electronic supplementary information (ESI) available: Analytical data and spectra (^1H and ^{13}C NMR), mass spectrometry data, CV curves and DFT calculation of configuration optimization materials, deposition numbers of single crystal of compound **4**. CCDC 993542. For ESI and crystallographic data in CIF or other electronic format see DOI: 10.1039/c4ob00873a

structures are gained *via* organogelation. In order to generate novel soft materials we synthesized new indolocarbazole derivatives *via* the Cadogan reactions (Scheme 1).[37–39] In the case of indolocarbazoles **4–6** without long carbon chains, the planar configuration of the polycyclic heterocycles would lead to extended π-conjugation, so strong π–π interactions would occur during the aggregation, which would not be favorable for the formation of the gel. As a result, crystals and crystal-like aggregates were formed from compounds **4–6.** In addition, we have previously found that *tert*-butyl could tune the strength of π–π interactions between carbazole units, and organogel could be obtained from *tert*-butyl substituted carbazoles directed by the balanced π–π interactions.[12,16] In order to decrease the strength of the π–π interactions between rigid indolocarbazole moieties, hexadecyl groups, which might enlarge the distance between conjugated units in the aggregates, were introduced. It is interesting that indolocarbazole derivatives with long alkyl groups **8–9** could form gels in alcohols (such as *tert*-amyl alcohol, *n*-octyl alcohol), acetone, DMSO, DMF and the mixed solvents containing methanol. The investigation of the gelation process revealed that the gelation ability of indolocarbazoles could be tuned by the structures of the π-skeletons. Herein, we provided a strategy to design π-gelators *via* tuning the π–π interactions between rigid conjugated systems. On the other hand, blue emitting gels are relatively rare, while in this work we fabricated the nanofibers with intense blue-light emission *via* organogelation of new indolocarbazoles. Notably, the fluorescence emission of the film based on xerogel **9** decreased significantly upon exposure to gaseous TNT, suggesting that the xerogels based on indolocarbazoles could become candidates as fluorescent sensory materials to detect vapors of explosives.

Results and discussion

Synthesis

The synthetic routes for the indolocarbazole derivatives without or with long carbon chains **4–9** are shown in Scheme 1. The reactions were performed under a N_2 atmosphere unless otherwise stated. Firstly, the boronic acids, including naphthalene-1,4-diyldiboronic acid, naphthalen-1-ylboronic acid and (4-(diphenylamino)phenyl)boronic acid, as well as 1,5-dibromo-2,4-dinitrobenzene were prepared according to the reported methods.[40–43] The double Suzuki–Miyaura cross coupling reaction between naphthalene-1,4-diyldiboronic acid and 1-bromo-2-nitrobenzene catalyzed by $Pd(PPh_3)_4$ in toluene–H_2O afforded compound **1** in a yield of 87%. Similarly, compounds **2** and **3** were synthesized *via* Suzuki–Miyaura reactions of 1,5-dibromo-2,4-dinitrobenzene with naphthalen-1-ylboronic acid or (4-(diphenylamino)phenyl)boronic acid in yields of 71% and 80%, respectively. Then, compounds **4–6** were obtained by Cadogan reactions through triethyl phosphate mediated reductive cyclization reactions of compounds **1–3** in yields of 42%, 12% and 13%, respectively. Finally, compounds **7–9** were obtained by the alkylation reactions of compounds **4–6** with 1-bromohexadecane catalyzed by NaH in yields of 85%, 76% and 72%, respectively. The obtained indolocarbazole derivatives were characterized by ^1H NMR, ^{13}C NMR, FT-IR and MALDI-TOF mass spectrometry. In addition, we attempted to obtain single crystals of compounds **4–6** by means of slow solvent diffusion. We found that after *n*-hexane was slowly diffused into the solutions of compounds **4–6** in THF, long rod-like crystals were obtained from compound **4**, needle-like crystals were generated from compound **5**, and thin plate crystals were obtained from compound **6**. Unfortunately, we only obtained the single crystal from compound **4**, while the X-ray diffraction signals of compounds **5** and **6** were too weak to be detected. As shown in Fig. 1, the

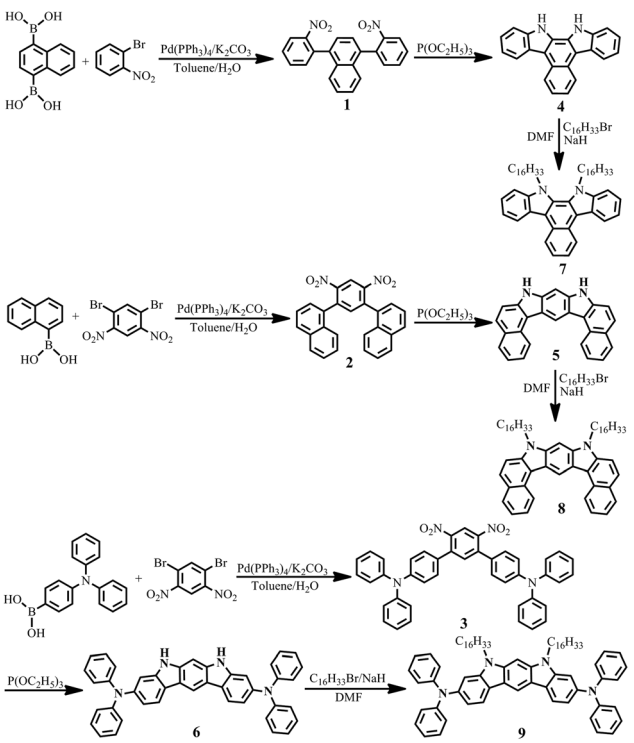

Scheme 1 Synthetic routes for the indolocarbazole derivatives.

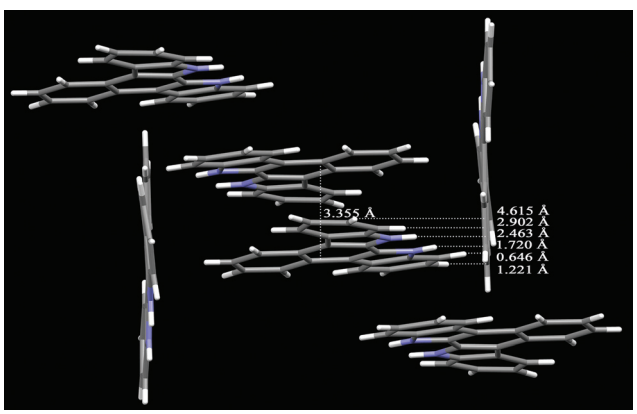

Fig. 1 Packing arrangement in the crystal structure of compound **4**.

molecule **4** exhibited good planarity and we could find a face to face stacking mode, in which the distance between two adjacent molecular planes was 3.355 Å. Additionally, we also found a vertically oriented stacking mode, in which the distances between H atoms and the vertical molecular plane were 0.646, 1.221, 1.720, 2.463, 2.902, and 4.615 Å, and the two N atoms in the aromatic ring were away from the molecular plane of 2.451 and 3.322 Å. The distances between H atoms connected to the N atom and the vertical molecular plane were 1.720 and 2.463 Å. It should be noted that the distance of 3.355 Å between the two indolocarbazole rings revealed that strong π–π interactions occurred in the single crystal of **4**.

UV-vis absorption and fluorescence emission spectra in solutions

The UV-vis absorption and fluorescence emission spectra of indolocarbazole derivatives **4–9** in THF (5×10^{-6} M) are shown in Fig. 2, and the data are listed in Table S1 (ESI†). The absorption behaviors of compounds **4–6** without long carbon chains are first discussed (Fig. 2a). It was clear that several well-resolved structured absorption bands appeared in the range of 250–420 nm for each compound. In detail, as to compound **4**, the absorption bands appeared in the range of 250–280 nm might be due to the B bands of benzene rings, and the absorption emerged at 345 nm and 362 nm might be ascribed to the electronic transitions from naphthalene and carbazole moieties. Similarly, for compound **5**, five absorption bands appeared in the UV region, such as 260 nm, 300 nm, 352 nm, 370 nm and 390 nm. The absorption at 300 nm and 352 nm could be attributed to π–π* transitions, and the absorption at 370 nm and 390 nm could be attributed to n–π* transitions. It should be noted that the absorption band at the long wavelength for compound **5** (390 nm) red-shifted compared with that for compound **4** (362 nm), indicating the enlarged conjugation length of **5**. Because of the introduction of triphenylamine units, the absorption band at the long wavelength for compound **6** (389 nm) red-shifted compared with compound **4**. The absorption bands for compound **6** at 289 nm and 321 nm could be attributed to π–π* transitions, while the absorption bands at 371 nm and 389 nm could be attributed to n–π* transitions. When long carbon chains were introduced into the N-positions of indolocarbazole derivatives, compounds **7–9** showed similar absorption behaviors to those of **4–6**, respectively, besides a small red-shift (less than 10 nm, Fig. 2b). For example, the absorption bands at 345 nm and 362 nm for compound **4** red-shifted to 352 nm and 369 nm for compound **7** because of the weak electron donating effect of carbon chains. As shown in Fig. 2c, compound **4** gave two strong emission bands at 367 nm and 386 nm, as well as a weak emission at 406 nm in THF (5×10^{-6} M) when excited at

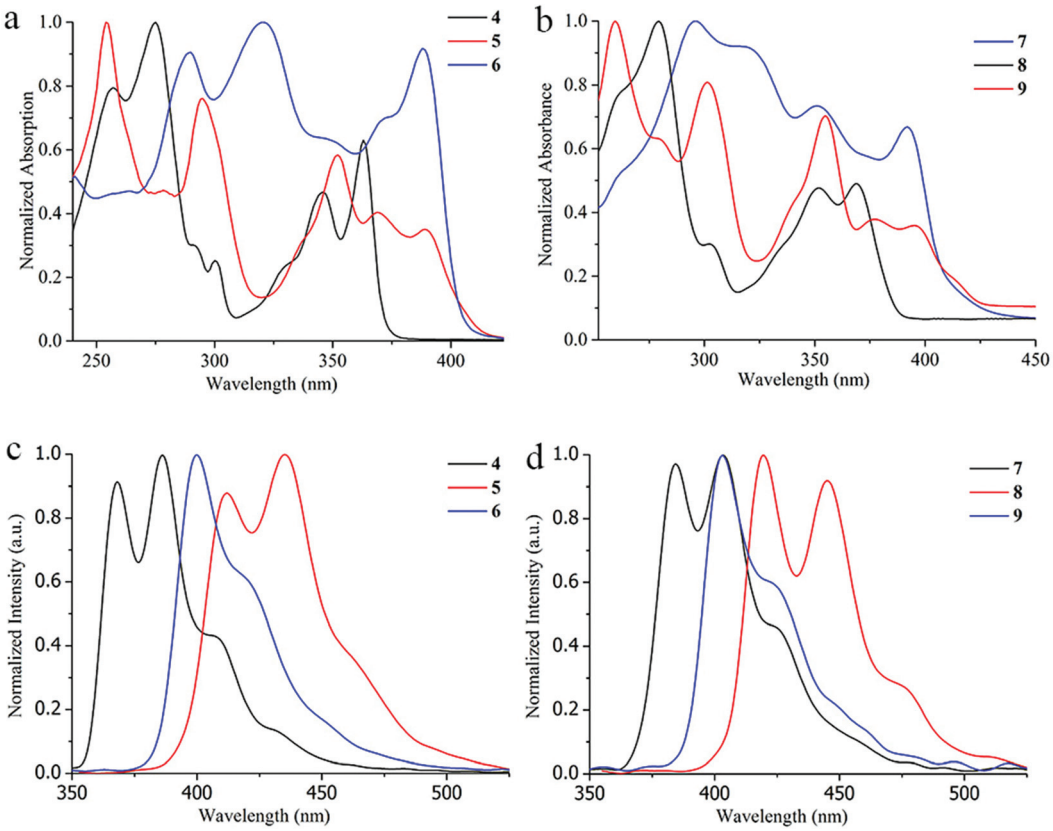

Fig. 2 Normalized UV-vis absorption (a, b) and fluorescence emission spectra (c, d) of compounds **4–9** in THF (5×10^{-6} M, λ_{ex} = 345 nm for compound **4**, λ_{ex} = 365 nm for compounds **5–9**).

345 nm. On account of the larger conjugation length of compound **5**, its emission in dilute solution red-shifted to 412 nm and 435 nm with a shoulder at *ca.* 460 nm (λ_{ex} = 365 nm) compared with compound **4**. In addition, a strong emission band at 400 nm with a shoulder at 418 nm was detected for compound **6**. Moreover, the fluorescence emission spectra of compounds **7–9** bearing long carbon chains were also similar to those of **4–7**, respectively, besides the red-shift (Fig. 2d). For instance, the strong emission bands of compound **8** shifted to 420 nm and 445 nm from 412 nm and 435 nm for compound **5** resulted from the weak electron donating ability of alkyl groups. The fluorescence quantum yields (Φ_F) of the synthesized indolocarbazole derivatives were determined in THF using quinine sulfate as the standard at room temperature (see Table S1†). The Φ_F values for compounds **4–9** were 0.44, 0.39, 0.66, 0.69, 0.38 and 0.45 respectively, meaning that they were high emissive in solutions.

Electrochemical properties and DFT calculations

Because the conjugated skeletons of indolocarbazole derivatives **4–6** were the same as those in **7–9**, respectively, the electrochemical properties of the selected compounds **7–9** were investigated using cyclic voltammetry with Ag/Ag^+ as the reference electrode in CH_2Cl_2. The electrochemical data and HOMO/LUMO energy levels are summarized in Table 1. Compounds **7** and **8** showed one reversible oxidation peak with onset potential around 1.2 V and 0.87 V, respectively, while compound **9** showed three reversible oxidation peaks with oxidation potentials around 0.69 V, 0.99 V and 1.33 V (see Fig. S2†). We deduced that the three oxidation peaks of compound **9** were originated from the oxidation processes of the indolocarbazole ring and two triphenylamine units, respectively, and the single oxidation peak for **7** and **8** without the triphenylamine moiety came from the oxidation of the indolocarbazole. The HOMO energy levels of compounds **7–9** calculated from the oxidation onset potential using the ferrocene calibrated formula of $E_{HOMO} = -(E^{ox}_{onset} + 4.19)$ eV were −5.39 eV, −5.06 eV and −4.9 eV, respectively, indicating strong electron donor abilities of the three compounds. The fluorescence quenching of compound **9** in the xerogel-based film when exposed to gaseous TNT could support this point, which will be discussed below. Since the reduction peaks were out of our scan range, the LUMO energy levels of compounds **7–9** were calculated from HOMO energy levels and the absorption band gaps, and they were −2.24 eV, −2.25 eV and −1.90 eV, respectively.

Moreover, the molecular orbitals and the optimized configurations of the synthesized indolocarbazole derivatives were studied by the B3LYP/6-31G level using the Gaussian 09w program. Based on the optimized molecular configurations we found that **4–6** without alkyl groups were planar molecules. When long alkyl groups were introduced to compounds **5** and **6**, the π-conjugated skeletons of compounds **8** and **9** were still in one plane because no interaction occurred between the two carbon chains (see Fig. S3–S4†). It meant that π–π interactions would occur during the aggregation of **8** or **9**, which might generate well-ordered arrangements. However, twist configuration of the aromatic heterocyclic ring was shown for compound **7**, in which the two long carbon chains extended to the front and back of the aromatic heterocyclic ring, respectively. We deemed that the steric hindrance of long carbon chains would affect its self-assembling properties. As shown in Fig. 3, the HOMO and LUMO for compounds **7–9** were mainly delocalized through the entire molecule besides the LUMO of **9** was delocalized over the indolocarbazole ring. In addition, the HOMO and LUMO energy levels obtained from the calculations are depicted in Table 1. It was clear that the calculated HOMO energy levels of compounds **7–9** were similar to those based on electrochemical results, and the HOMO energy level of **7** was lower than compounds **8** and **9**. As to the calculated LUMO energy levels for compounds **7–9**, although they were higher than the data from electrochemical results, they were in the same order of **9** > **7** > **8** as that based on electrochemical data.

Gelation properties

We found that the indolocarbazole derivatives **4–6** could not form any organogels due to their strong π–π interactions during aggregation. In order to gain new indolocarbazole-based organogels, long carbon chains were introduced to compounds **4–6**, which would adjust the balance between the solubility and precipitation in organic liquids. As shown in Table 2, compounds **8** and **9** could form opacity gels in polar solvents, including acetone, *tert*-amyl alcohol, *n*-octyl alcohol, DMSO, DMF and the mixed solvents containing methanol, such as dichloromethane–methanol (v/v = 1/1), 1,2-dichloroethane–methanol (v/v = 1/1), chloroform–methanol (v/v = 1/1), tetrahydrofuran–methanol (v/v = 1/1), toluene–methanol, diethyl ether–methanol, ethyl acetate–methanol under ultra-

Table 1 Electrochemical data and HOMO/LUMO energy levels of compounds **7–9**

Compound	E^{ox}_{onset} (V)[a](eV)	HOMO[b] (eV)	LUMO[b] (eV)	E_g[c] (eV)	HOMO[d] (eV)	LUMO[d] (eV)
7	1.20	−5.39	−2.24	3.15	−5.32	−1.10
8	0.87	−5.06	−2.25	2.81	−4.74	−1.14
9	0.69	−4.90	−1.90	3.00	−4.72	−0.79

[a] E^{ox}_{onset} (V) = onset oxidation potential; potentials *versus* Ag/Ag^+, working electrode Pt, 0.1 M Bu_4NPF_6–CH_2Cl_2, scan rate 50 mV/S, Fc^+/Fc was used as an external reference. [b] $E_{HOMO} = -(E^{ox}_{onset} + 4.19)$ eV; LUMO = HOMO + E_g. [c] Determined from the onset of the absorption at the lower energy band edge ($E_g = 1240/\lambda_{onset}$). [d] Calculated data.

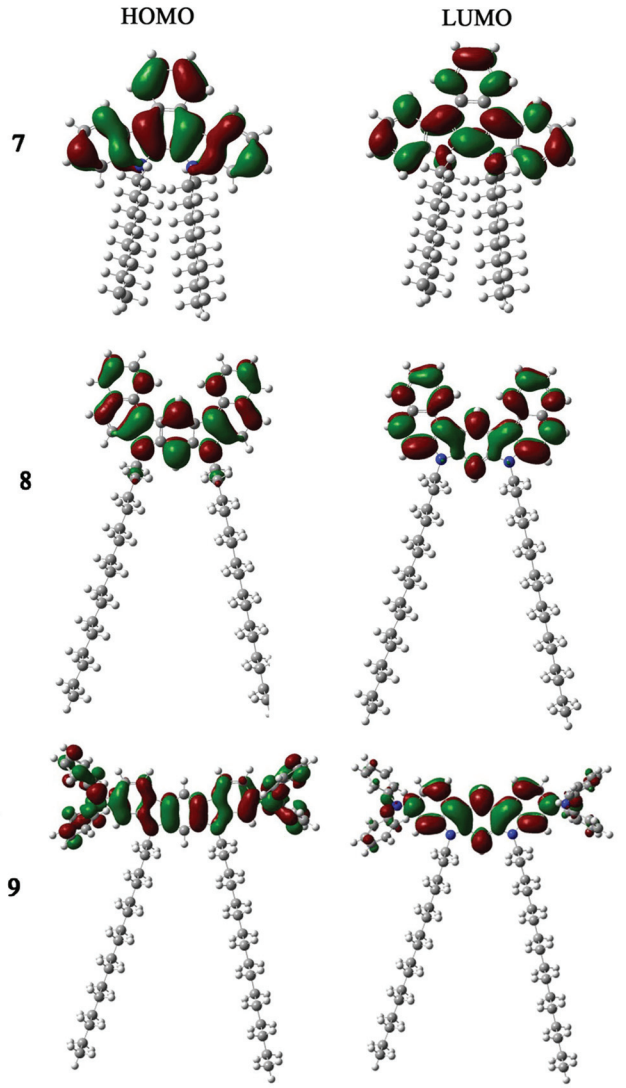

Fig. 3 The molecular orbital surfaces of HOMO and LUMO for compounds **7–9** calculated by the B3LYP/6-31G method using the Gaussian 09w program.

sound stimulation. The low critical gelation concentrations (CGC) for compounds **8** and **9** in the above solvents were in the range of 3.1–12.4 mM and 0.6–3.8 mM, respectively. Therefore, we could deduce that the gel formation ability of compound **9** was stronger than **8**, and **9** could be considered as a supergelator to some extent.[13] The obtained gels were stable for several months at room temperature and could be destroyed when heated. Moreover, the organogels could be recovered after the hot solutions were stimulated by ultrasound. Although the indolocarbazole ring was involved in compound **7**, no organogel was obtained because the two long carbon chains extended to the front and back of the slight twist aromatic heterocyclic ring, respectively (Fig. S4†). The steric hindrance of long carbon chains in compound **7** would prevent the occurrence of π–π interactions between indolocarbazole units, which would be unfavorable for the gelation. Therefore, it was understandable that compound **7** could be

Table 2 Gelation abilities of compounds **7–9** in organic solvents

Solvent	7	8 (CGC[a]/mM)	9 (CGC/mM)
Methanol	P	PG	P
Ethanol	P	PG	P
Acetone	S	G (4.1)	G (2.1)
Acetonitrile	P	P	P
tert-Amyl alcohol	P	G (12.4)	G (1.4)
Glycol dimethyl ether	P	S	S
Glycol	P	P	P
n-Octyl alcohol	P	G (5.0)	G (1.9)
DMSO	S	G (9.9)	G (2.1)
DMF	S	G (7.1)	G (1.1)
Dichloromethane–methanol	S	(v/v = 1/1) G (3.1)	(v/v = 1/1) G (2.7)
1,2-Dichloroethane–methanol	S	(v/v = 1/1) G (3.3)	(v/v = 1/1) G (1.9)
Toluene–methanol	S	(v/v = 1/1) G (4.2)	(v/v = 1/2) G (0.9)
Chloroform–methanol	S	(v/v = 1/1) G (4.9)	(v/v = 1/1) G (3.8)
Diethyl ether–methanol	S	(v/v = 2/1) G (5.5)	(v/v = 1/1) G (1.5)
THF–methanol	S	(v/v = 1/1) G (3.0)	(v/v = 1/1) G (2.6)
Ethyl acetate–methanol	S	(v/v = 2/1) G (5.6)	(v/v = 1/1) G (0.6)

P = precipitate; PG = partly gel; S = soluble; G = gel. [a] CGC: critical gelation concentration.

easily dissolved in most common solvents, including dichloromethane, chloroform, ethyl acetate, THF, DMF, DMSO, *etc.* In the cases of compounds **8** and **9**, the long carbon chains extended in the same plane of indolocarbazoles, so the conjugated moieties could approach each other and π–π interactions might become the driving force for the gel formation, which was confirmed by the UV-vis absorption and fluorescence emission spectral changes during the gelation processes.

The morphologies of xerogels **8** and **9** obtained from DMSO were investigated by SEM. As shown in Fig. 4, lots of long fibers with diameters of 6–18 μm were formed from **8** in DMSO gel, while the formed fibers in xerogel **9** were more slender, whose diameter was in the range of 1.5–4.1 μm. We also found that most of the fibers in xerogel **9** were made up of several thinner fibers, which twined together to form many junctions.

In order to investigate the process of gel formation, the time-dependent UV-vis absorption and fluorescence emission spectra of compounds **8** and **9** in DMSO upon cooling the hot solutions, which were stimulated with ultrasound for 5 s, to room temperature are shown in Fig. 5. It was found that during the gel formation of compound **8** the absorption bands decreased gradually. It should be noted that the n–π* transition band at 398 nm in hot solution red-shifted to 402 nm in the gel state, indicating the formation of J-aggregates in the gel state. However, during the gel formation of compound **9** the UV-vis absorption spectra showed abnormal changes. When the hot solution was naturally cooled down within 40 s (the gel was not formed), the absorption bands decreased gradually because the solution became a bit of opaque. Further prolong-

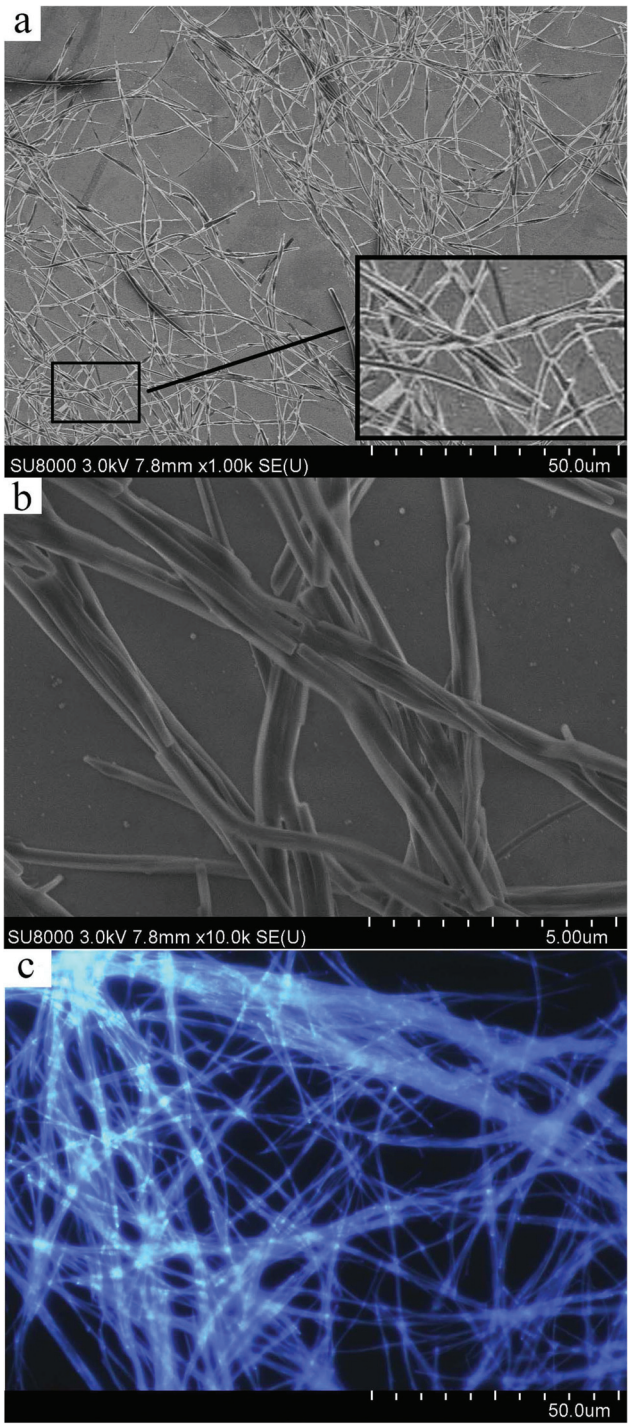

Fig. 4 SEM images for the xerogels **8** (b, 9.9×10^{-3} M) and **9** (a, 6.4×10^{-3} M), and fluorescence microscopy for xerogel **9** (c, 6.4×10^{-3} M, λ_{ex} = 365 nm) obtained from DMSO.

ing the cooling time, the absorption band at 298 nm increased gradually, and the two bands at 330 nm and 356 nm combined into one at 350 nm, which also increased during the gel formation. Such spectral changes indicated the occurrence of the π–π interaction in the gelation process. In addition, the absorption band at 411 nm in hot solution blue-shifted obviously during the cooling process, and shifted to 403 nm in the gel state. It suggested that the H-aggregates were formed in the gel state of compound **9**. From the time-dependent fluorescence emission spectra we could find that the emission intensities of compounds **8** and **9** decreased significantly upon cooling the hot solutions to room temperature. Meanwhile, the emission band for compound **9** blue-shifted from 418 nm in solution to 416 nm in the gel state, and no shift was detected during the gel formation of **8**. The above changes of the emission spectra indicated that π–π interactions played a key role in the gel formation. Notably, although the fluorescence emission intensity of compounds **8** and **9** decreased during the gel formation to some extent, the organogels still emitted strong blue light (Fig. 4c). As a result, the nanofibers with strong blue-light emission were obtained *via* the organogelation of the indolocarbazole derivative, which might become candidates as fluorescent sensory and emitting materials.

In order to reveal the stacking mode of compounds **8** and **9** in gel phases, we showed the XRD patterns of the xerogels in Fig. 6. The xerogel **8** gave three diffraction peaks in small angle area, and the corresponding *d*-spacing values were 2.2 nm, 1.1 nm and 0.87 nm, respectively, corresponding to a ratio of 1 : 1/2 : 1/3 (Fig. 6a). It indicated that a layered structure with a long period of 2.2 nm was generated from molecule **8** in the gel state. Combined with the optimized molecular length of molecule **8** (2.3 nm) based on the semiempirical (AM1) calculations (see Fig. S1a†) we suggested that the molecule **8** arranged into a lamellar structure using the molecular length as the long period in the gel state. Moreover, in the wide angle region of the XRD pattern for xerogel **8** we could detect the diffraction peaks with *d*-spacings of 0.41 nm and 0.37 nm (see the inset in Fig. 6a), and the latter one was the typical distance between aromatic rings in π-aggregates. It could further confirm the formation of π-aggregates in the gel phase of **8**, which was in accordance with the results of time-dependent UV-vis absorption and emission spectral data. In addition, the diffraction peak with a *d*-spacing of 0.41 nm was suggested as the distance between the neighboring long carbon chains. Therefore, we proposed the possible molecular packing model for compound **8** in the gel phase as shown in Fig. 6b, in which the molecular plane and alkyl chain adopted a parallel stacking mode and J-aggregates were involved. Additionally, the xerogel **9** showed two diffraction peaks in the small angle area and the corresponding *d*-spacings were 3.1 nm and 1.0 nm with a ratio of *ca.* 1 : 1/3 (see Fig. 6c). Although the second diffraction peak could not be detected, we could deduce that molecule **9** adopted a layered structure with a long period of 3.1 nm in the gel state. The result of the semiempirical (AM1) calculations showed that the length of molecule **9** was 2.1 nm (see Fig. S1b†), so we suggested that the stacking mode in xerogel **9** adopted a bimolecular layered structure. The wide angle XRD pattern of xerogel **9** showed two diffraction peaks with *d*-spacings of 0.42 nm and 0.39 nm (see the inset in Fig. 6c). The latter one could be ascribed to the distance between aromatic planes and the former one corresponded to the distance between long carbon chains. Therefore, a layered

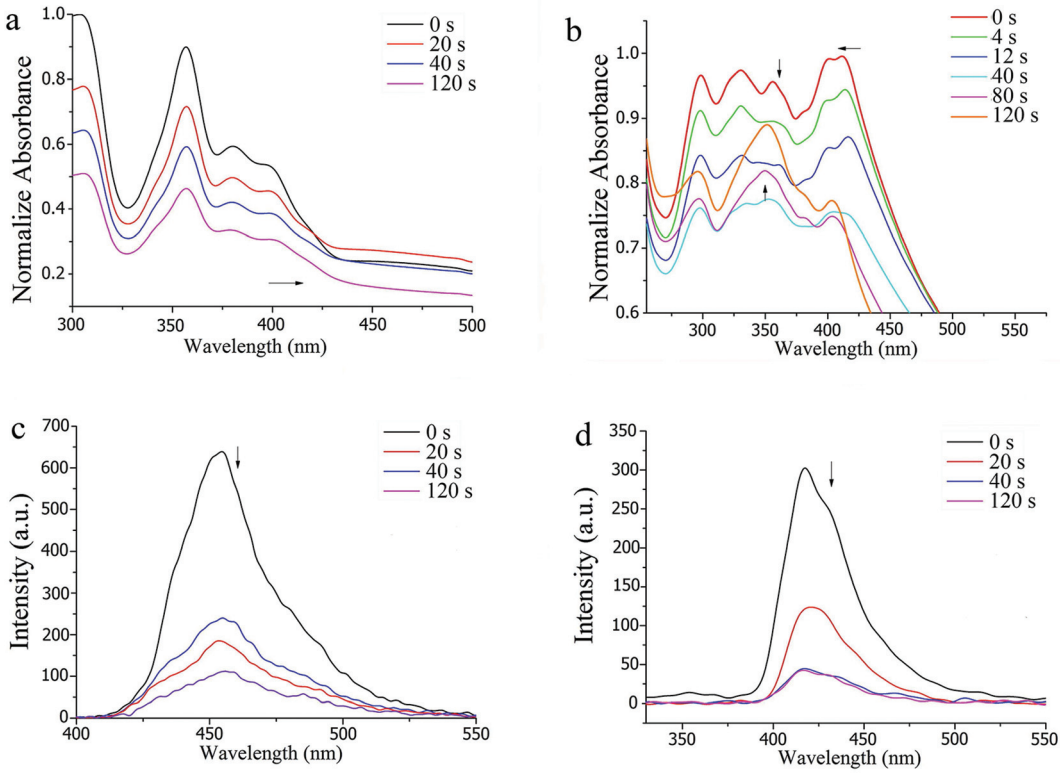

Fig. 5 UV-vis absorption (a for **8**, b for **9**) and fluorescence emission (c for **8**, d for **9**) spectra of **8** (9.9×10^{-3} M) and **9** (6.4×10^{-3} M) during the gelation process in DMSO.

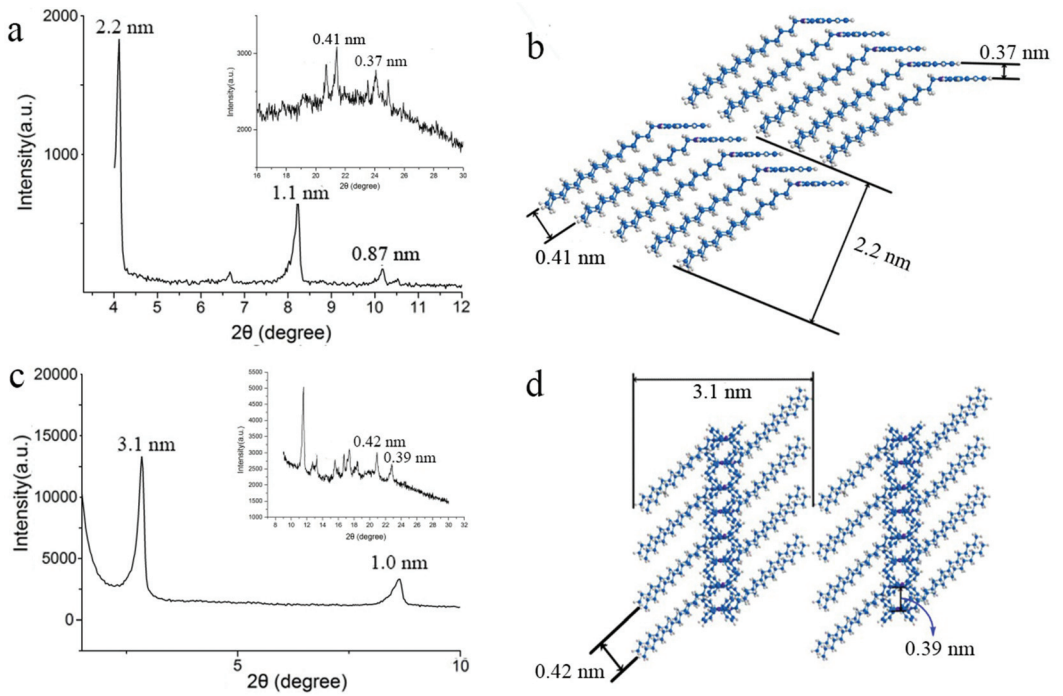

Fig. 6 XRD patterns of the xerogels **8** (a) and **9** (c) obtained from DMSO, and the proposed molecular packing models of **8** (b) and **9** (d) in gel phases.

structure was proposed for the molecular packing model for compound **9** in the gel state as shown in Fig. 6d, in which H-aggregates were formed, according to the results based on the absorption spectral changes during sol–gel transition. It should be noted that the distance between aromatic rings in xerogel **8** was shorter than that in **9**, meaning that stronger π–π interactions would happen in gel **8** than in **9**. The stronger the π–π interactions, the easier the crystallization of the conjugated molecule. In our case, the gelation ability of compound **9** was better than compounds **7** and **8** might be attributed to the balanced π–π interactions. Therefore, it is useful for the fabrication of π-gels with desired functionality by tuning the strength of π–π interactions in the aggregated states.

Fluorescent sensory properties of compound 9 in the xerogel-based film for probing gaseous TNT

On the one hand, the detection of explosives is important in military operations and public security, and some emitting electron-rich conjugated systems can sense aromatic nitro compounds *via* fluorescence quenching.[44,45] On the other hand, we have found that the synthesized indolocarbazoles were electron donors and strongly emissive in the xerogel-based film. Therefore, we selected xerogel **9** as an example to study its fluorescent sensory properties for detecting TNT (2,4,6-trinitrotoluene). As shown in Fig. 7, the fluorescence emission intensity of compound **9** in xerogel-based film decreased significantly upon exposure to gaseous TNT at 40 °C, and the fluorescence quenching efficiency reached 62% when the exposure time was 5 min. We deduced that the good sensitivity of the xerogel-based film of compound **9** towards TNT resulted from the amplified fluorescence quenching induced by the enhanced intermolecular exciton diffusion along the long axis of the 1D nanofibers as well as the high surface-to-volume ratio and the large interspace in 3D networks.[13,15]

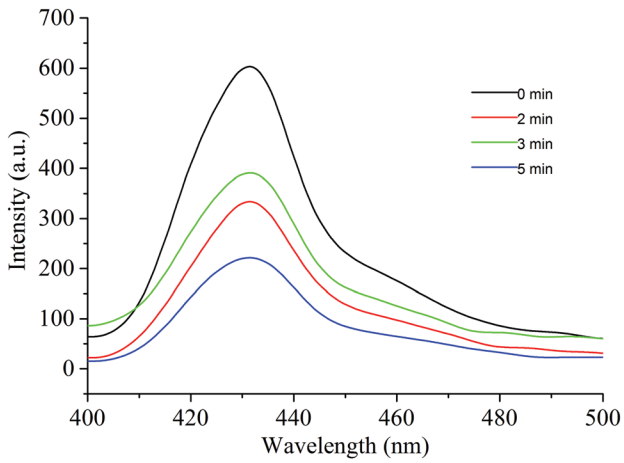

Fig. 7 Time-dependent fluorescence emission spectra of compound **9** in xerogel-based film upon exposure to the saturated vapor of TNT at 40 °C (λ_{ex} = 365 nm).

Conclusions

In summary, new indolocarbazole derivatives with extended π-conjugated systems **4–9** have been synthesized. It was found that the indolocarbazole derivatives could emit strong blue light in solutions and in gel states. The indolocarbazoles without long carbon chains **4–6** tended to form crystal or crystal-like aggregates due to strong π–π interactions. It should be noted that the strength of π–π interactions could be reduced to some extent *via* the introduction of long alkyl groups into N-positions of indolocarbazoles. As a result, the organogels based on indolocarbazoles were gained in alcohols (such as *tert*-amyl alcohol, *n*-octyl alcohol and the mixed solvents containing methanol), acetone and DMSO, directed by balanced π–π interactions. The molecular packing models of indolocarbazoles were proposed, and the layered structures were involved in the nanostructures. Notably, the xerogel-based film of compound **9** could sense gaseous TNT with high sensitivity *via* fluorescence quenching because the amplified fluorescence quenching could be induced by the enhanced intermolecular exciton diffusion along the long axis of the 1D nanofibers and the high surface-to-volume ratio and large interspace in the 3D networks favored the adsorption, accumulation and diffusion of gaseous molecules. It is believed that the gelation of polycyclic aromatic heterocyclic compounds is useful for the construction of novel functional soft materials, exhibiting unique photophysical and optoelectronic properties.

Experimental

Instruments

^{1}H NMR spectra were recorded with a Bruker avance III 500 or avance III 400 MHz using $CDCl_3$ and DMSO-d_6 as the solvents. ^{13}C NMR spectra were recorded on a mercury plus 125 MHz or 100 MHz using $CDCl_3$ and DMSO-d_6 as the solvents. Mass spectra were performed on Agilent 1100 MS series and AXIMA CFR MALDI/TOF (matrix assisted laser desorption ionization/time-of-flight) MS (COMPACT). IR spectra were measured with a Nicolet-360 FT-IR spectrometer by incorporation of samples in KBr disks. UV-vis absorption spectra were determined on a Shimadzu UV-1601PC Spectrophotometer. Fluorescence emission spectra were carried out on a Shimadzu RF-5301 Luminescence Spectrometer. Fluorescence microscopy images were obtained on a fluorescence microscope (Olympus Reflected Fluorescence System BX51, Olympus, Japan). SEM images were obtained through the HITACHI-SU8020. XRD spectra were determined on the PANalytical-Empyrean. Cyclic voltammetry (CV) was performed using a CHI 604C voltammetric analyzer and measurements were carried out in CH_2Cl_2 (refluxed with CaH_2 overnight) containing 0.1 M Bu_4NBF_4 as a supporting electrolyte. A platinum button was used as a working electrode and a platinum plate as a counter electrode. All potentials were recorded versus Ag/Ag^+ as a reference electrode (using ferrocene as an internal standard). The scan rate was maintained at 50 mV s^{-1}. The optimized configurations and HOMO

and LUMO molecular orbitals were calculated by the DFT (B3LYP/6-31G) method on the Gaussian 09 software.

Fabrication of organogel and xerogel-based film

The solutions of indolocarbazoles in selected organic solvents were obtained by heating. After the hot solutions were subjected to sonication for 5 s, followed by aging at room temperature, the organogels were formed. The xerogel-based film was generated by dropping the organogel **9** (obtained from DMSO) dispersed in ethanol on a glass slide, followed by the natural evaporation of the solvent.

Sensing properties of compound 9 in the xerogel-based film

The sensing performance of compound **9** in the xerogel-based film towards vapor of TNT was studied in a way adopted by Swager.[46] The film to be tested was inserted into a sealed vial containing solid TNT and cotton gauze, which could prevent the direct contact of the film and the analyte, at 40 °C. The time-dependent fluorescence spectra of the film were measured after immersing the film into the sealed vial for a certain time.

Materials

The precursors of naphthalene-1,4-diyldiboronic acid, naphthalen-1-ylboronic acid, (4-(diphenylamino)phenyl)-boronic acid and the 1,5-dibromo-2,4-dinitrobenzene were synthesized according to the literature.[40–43]

1,4-Bis(2-nitrophenyl)naphthalene (1). A mixture of 1-bromo-2-nitrobenzene (4.65 g, 23 mmol), naphthalene-1,4-diyldiboronic acid (2.00 g, 9.27 mmol), sodium carbonate (9.00 g, 65 mmol), water (30 mL) and toluene (30 mL) was first refluxed under a N_2 atmosphere, and $Pd(PPh_3)_4$ (0.04 g, 0.03 mmol) was added rapidly. After refluxing for 2 days, the organic layer was separated. After drying over anhydrous magnesium sulfate, the solvent was removed. The crude product was purified by column chromatography using petroleum ether–ethyl acetate (v/v = 5/1) as an eluent to afford **1** (3.00 g, 87%) as yellow powder. mp > 200 °C. ^{1}H NMR (400 MHz, $CDCl_3$) (ppm): 8.10 (d, 2H, J = 8.1 Hz), 7.74 (d, 2H, J = 7.74 Hz), 7.65 (m, 2H), 7.59 (m, 2H, ArH), 7.51 (m, 2H, ArH), 7.41 (m, 2H, ArH), 7.37 (s, 2H, ArH) (see Fig. S5†). IR (KBr, cm^{-1}): 3057, 2922, 2858, 1950, 1869, 1834, 1741, 1518, 1340, 849, 771. MS, m/z: calc.: 370.1, found: 369.5 [M^+] (see Fig. S6†).

1,1′-(4,6-Dinitro-1,3-phenylene)dinaphthalene (2). By following the synthetic procedure for compound **1** except naphthalen-1-ylboronic acid (3.00 g, 17.4 mmol) and 1,5-dibromo-2,4-dinitrobenzene (2.84 g, 8.7 mmol) as reagents. The crude product was purified by column chromatography using petroleum ether–ethyl acetate (v/v = 5/1) as an eluent to afford **2** (2.60 g, 71%) as yellow powder. mp > 200 °C. ^{1}H NMR (400 MHz, $CDCl_3$) (ppm): 8.85 (d, 1H, J = 8.85 Hz), 7.93 (t, 4H, J = 7.94 Hz), 7.70 (d, 1H, ArH), 7.52 (m, 8H, ArH), 7.42 (dd, 2H, J = 7.43 Hz) (see Fig. S7†). IR (KBr, cm^{-1}): 3049, 2862, 1936, 1815, 1722, 1589, 1522, 1346, 918, 775. MS, m/z: calc.: 420.4, found: 419.6 [M^+] (see Fig. S8†).

4′,6′-Dinitro-N^4,N^4,$N^{4''}$,$N^{4''}$-tetraphenyl-[1,1′:3′,1″-terphenyl]-4,4″-diamine (3). By following the synthetic procedure for compound **1** except (4-(diphenylamino)phenyl)boronic acid (2.00 g, 6.90 mmol) and 1,5-dibromo-2,4-dinitrobenzene (1.20 g, 3.68 mmol) as reagents. The crude product was purified by column chromatography using petroleum ether–ethyl acetate (v/v = 4/1) as an eluent to afford **3** (1.80 g, 80%) as red powder. mp > 200 °C. ^{1}H NMR (400 MHz, $CDCl_3$) (ppm): 8.36 (s, 1H, ArH), 7.55 (s, 1H, ArH), 7.30 (t, 8H, J = 7.30 Hz), 7.16 (m, 12H, ArH), 7.08 (m, 8H, ArH) (see Fig. S9†). IR (KBr, cm^{-1}): 3039, 2924, 1589, 1520, 1493, 1335, 1282, 1184, 831, 754, 698, 517. MS, m/z: calc.: 654.7, found: 655.3 [M^+ + H] (see Fig. S10†).

13,14-Dihydrobenzo[*c*]indolo[2,3-*a*]carbazole (4). A solution of **1** (2.00 g, 5.4 mmol) in triethyl phosphite (20 mL) was refluxed for 2 days under a N_2 atmosphere. After triethyl phosphite was evaporated under vacuum, the residue was purified by column chromatography using dichloromethane as an eluent to afford **4** (0.70 g, 42%) as a light yellow solid. mp > 200 °C. ^{1}H NMR (400 MHz, DMSO-d_6) δ (ppm): 11.56 (s, 2H, NH), 8.91 (s, 2H, ArH), 8.64 (d, 2H, ArH, J = 8.64 Hz), 7.83 (d, 2H, ArH, J = 7.83 Hz), 7.66 (m, 2H, ArH), 7.45 (t, 2H, ArH, J = 7.45 Hz), 7.36 (t, 2H, ArH, J = 7.36 Hz) (see Fig. S11†). ^{13}C NMR (100 MHz, DMSO-d_6) δ (ppm): 138.40, 126.45, 125.93, 123.95, 123.75, 123.59, 121.26, 120.12, 113.22, 112.19 (see Fig. S12†). IR (KBr, cm^{-1}): 3408, 3049, 1622, 1545, 1421, 1327, 1261, 744, 663, 428. MS, m/z: calc.: 306.4, found: 307.4 [M^+ + H] (see Fig. S13†).

7,9-Dihydrobenzo[*g*]benzo[4,5]indolo[2,3-*b*]carbazole (5). By following the synthetic procedure for compound **4** except using compound **2** (2.00 g, 0.78 mmol) and triethyl phosphite as reagents. After triethyl phosphite was evaporated under vacuum, the residue was recrystallized in THF and petroleum ether to afford the crude product as a dark brown solid, which was further purified by column chromatography using dichloromethane as an eluent to afford **5** (0.20 g, 12%) as a light yellow solid, mp > 200 °C. ^{1}H NMR (400 MHz, DMSO-d_6) δ (ppm): 11.67 (s, 2H, NH), 9.57 (s, 1H, ArH), 9.11 (d, 2H, ArH, J = 9.10 Hz), 8.11 (d, 2H, ArH, J = 8.09 Hz), 7.94 (d, 2H, ArH, J = 7.93 Hz), 7.89 (t, 2H, ArH, J = 7.87 Hz), 7.82 (s, 1H, ArH), 7.79 (d, 2H, ArH, J = 7.77 Hz), 7.53 (t, 2H, ArH, J = 7.51 Hz) (see Fig. S14†). ^{13}C NMR (100 MHz, DMSO-d_6) δ (ppm): 138.69, 138.64, 129.73, 129.64, 128.91, 127.48, 126.60, 123.52, 122.77, 119.62, 114.73, 113.71, 113.64 (see Fig. S15†). IR (KBr, cm^{-1}): 3406, 3053, 2931, 1618, 1521, 1460, 1319, 1167, 1018, 810, 740, 451. MS, m/z: calc.: 356.4, found: 357.6 [M^+ + H] (see Fig. S16†).

N^3,N^3,N^9,N^9-Tetraphenyl-5,7-dihydroindolo[2,3-*b*]carbazole-3,9-diamine (6). By following the synthetic procedure for compound **4** except using compound **3** (1.00 g, 1.53 mmol) and triethyl phosphite as reagents. After triethyl phosphite was evaporated under vacuum, the residue was purified by column chromatography using dichloromethane as an eluent, followed by recrystallization from light petroleum to afford **6** (0.12 g, 13%) as a brown solid. mp > 200 °C. ^{1}H NMR (400 MHz, DMSO-d_6) δ (ppm): 10.9 (s, 2H, NH), 8.64 (s, 1H, ArH), 8.05 (d,

2H, ArH, J = 8.04 Hz), 7.30 (t, 9H, ArH, J = 7.29 Hz), 7.04 (m, 14H, ArH, J = 7.02 Hz), 6.86 (d, 2H, ArH, J = 6.85 Hz) (see Fig. S17†). ^{13}C NMR (100 MHz, DMSO-d_6) δ (ppm):148.41, 144.80, 141.77, 140.65, 129.83, 123.67, 122.72, 120.57, 120.04, 117.78, 116.71, 110.68, 107.23 (see Fig. S18†). IR (KBr, cm^{-1}): 3400, 3030, 2955, 2862, 1601, 1477, 833, 746, 683, 472. MS, m/z: calc.: 590.7, found: 592.1 [M^+ + 2H] (see Fig. S19†).

13,14-Dihexadecyl-13,14-dihydrobenzo[*c*]indolo[2,3-*a*]carbazole (7). A solution of compound **4** (0.20 g, 0.65 mmol) and $C_{16}H_{33}Br$ (0.50 g,1.63 mmol) in DMF was cooled by ice-water to 0 °C and NaH (0.10 g, 4.2 mmol) was slowly added under a N_2 atmosphere. After stirring at room temperature for 2 hours, the mixture was poured into ice water and extracted by CH_2Cl_2. The organic phase was washed with brine and dried over anhydrous magnesium sulfate. After CH_2Cl_2 was removed, the crude product was purified by column chromatography using dichloromethane–petroleum (v/v = 1/7) as an eluent to afford **7** (0.42 g, 85%) as a white solid. mp = 68.0–69.0 °C. ^{1}H NMR (400 MHz,$CDCl_3$) δ (ppm): 8.95 (dd, 2H, ArH, J = 8.95 Hz), 8.66 (d, 2H, ArH, J = 8.66 Hz), 7.67 (dd, 4H, ArH, J = 7.68 Hz), 7.50 (t, 2H, ArH, J = 7.50 Hz), 7.43 (t, 2H, ArH, J = 7.43 Hz), 4.66 (t, 4H, $NC_{16}H_{33}$, J = 4.66 Hz), 1.77 (m, 4H, $NC_{16}H_{33}$, J = 1.8 Hz), 1.42 (m, 4H, $NC_{16}H_{33}$, J = 1.41 Hz), 1.26 (m, 48H, $NC_{16}H_{33}$), 0.88 (t, 6H, $NC_{16}H_{33}$, J = 0.87 Hz) (see Fig. S20†). ^{13}C NMR (100 MHz, $CDCl_3$) δ (ppm): 143.02, 131.01, 127.05, 127.13, 124.03, 123.91, 123.88, 122.15, 121.09, 118.19, 112.48, 48.39, 31.96, 29.72, 29.69, 29.66, 29.60, 29.52, 29.40, 29.28, 28.89, 22.73, 14.16, 0.03 (see Fig. S21†). IR (KBr, cm^{-1}): 2929, 2848, 1628, 1531, 1452, 1335, 748. MS, m/z: calc.: 754.6, found: 756.2 [M^+ + H] (see Fig. S22†).

7,9-Dihexadecyl-7,9-dihydrobenzo[*g*]benzo[4,5]indolo[2,3-*b*]carbazole (8). By following the synthetic procedure for compound **7** except using **5** (0.20 g, 0.56 mmol), $C_{16}H_{33}Br$ (0.43 g, 1.4 mmol) and NaH (0.10 g, 4.2 mmol) as reagents. The crude product was purified by column chromatography using dichloromethane–petroleum (v/v = 1/7) as an eluent to afford **8** (0.34 g, 76%) as a brown solid. mp = 106.0–108.0 °C. ^{1}H NMR (400 MHz, $CDCl_3$) δ (ppm): 9.76 (s, 1H, ArH), 9.11 (d, 2H, ArH, J = 9.11 Hz), 8.07 (d, 2H, ArH, J = 8.07 Hz), 7.93 (d, 2H, ArH, J = 7.93 Hz), 7.89 (t, 2H, ArH, J = 7.89 Hz), 7.71 (d, 2H, ArH, J = 7.71 Hz), 7.53(dd, 2H, ArH, J = 7.52 Hz), 7.47 (s, 1H, ArH), 4.55 (t, 4H, $NC_{16}H_{33}$, J = 4.55 Hz), 2.02 (m, 4H, $NC_{16}H_{33}$, J = 2.02 Hz), 1.48 (m, 4H, $NC_{16}H_{33}$, J = 1.47 Hz), 1.37 (m, 4H, $NC_{16}H_{33}$, J = 1.37 Hz), 1.22 (m, 44H, $NC_{16}H_{33}$, J = 1.24 Hz), 0.87 (t, 6H, $NC_{16}H_{33}$, J = 0.87 Hz) (see Fig. S23†). ^{13}C NMR (100 MHz, $CDCl_3$) δ (ppm): 138.83, 138.69, 129.82, 129.31, 128.86, 126.90, 126.16, 123.11, 122.50, 119.31, 115.21, 115.01, 110.58, 87.82, 43.24, 31.96, 29.74, 29.71, 29.59, 29.40, 22.73, 14.17, 0.03 (see Fig. S24†). IR (KBr, cm^{-1}): 2924, 2850, 1628, 1468, 1323, 793, 731. MS, m/z: calc.: 804.6, found: 805.8 [M^+ + H] (see Fig. S25†).

5,7-Dihexadecyl-N^3,N^3,N^9,N^9-tetraphenyl-5,7-dihydroindolo-[2,3-*b*]carbazole-3,9-diamine (9). By following the synthetic procedure for compound **7** except using compound **6** (0.20 g, 0.34 mmol), $C_{16}H_{33}Br$ (0.26 g, 0.85 mmol) and NaH (0.10 g, 4.2 mmol) as reagents. The crude product was purified by column chromatography using dichloromethane–petroleum (v/v = 1/7) as an eluent to afford **9** (0.25 g, 72%) as a light yellow solid. mp = 121.0–123.0 °C. ^{1}H NMR (400 MHz,$CDCl_3$) δ (ppm): 8.55 (s, 1H, ArH), 8.01 (d, 2H, ArH, J = 8.01 Hz), 7.25 (m, 8H, ArH, J = 7.25 Hz), 7.15 (m,10H, ArH, J = 7.15 Hz), 7.06 (s, 1H, ArH), 6.99 (t, 6H, ArH, J = 6.99 Hz), 4.19 (t, 4H, $NC_{16}H_{33}$, J = 4.20 Hz), 1.81 (m, 4H, $NC_{16}H_{33}$, J = 1.81 Hz), 1.24 (m, 52H, $NC_{16}H_{33}$, J = 1.24 Hz), 0.87 (m, 6H, $NC_{16}H_{33}$, J = 0.86 Hz) (see Fig. S26†). ^{13}C NMR (100 MHz, $CDCl_3$) δ (ppm): 148.46, 145.05, 142.05, 141.09, 129.11, 123.54, 122.09, 120.09, 119.73, 117.50, 117.22, 110.61, 105.47, 87.01, 43.08, 29.75, 29.71, 29.59, 29.54, 29.41, 22.74, 14.18 (see Fig. S27†). IR (KBr, cm^{-1}): 2920, 2854, 1601, 1456, 1321, 1259, 1117,746, 694. MS, m/z: calc.: 1038.8, found: 1039.9 [M^+ + H] (see Fig. S28†).

Acknowledgements

This work was financially supported by the National Natural Science Foundation of China (21374041) and the Open Project of State Key Laboratory of Supramolecular Structure and Materials (SKLSSM201407) and the Open Project of State Key Laboratory of Theoretical and Computational Chemistry (K2013-02).

Notes and references

1 X. F. Zhang, R. Lu, J. J. Jia, X. L. Liu, P. C. Xue, D. F. Xu and H. P. Zhou, *Chem. Commun.*, 2010, **46**, 8419–8421.
2 M. George and R. G. Weiss, *Acc. Chem. Res.*, 2006, **39**, 489–497.
3 A. R. A. Palmans and E. W. Meijer, *Angew. Chem., Int. Ed.*, 2007, **46**, 8948–8968.
4 P. Chen, R. Lu, P. C. Xue, T. H. Xu, G. J. Chen and Y. Y. Zhao, *Langmuir*, 2009, **25**, 8395–8399.
5 C. Y. Bao, R. Lu, M. Jin, P. C. Xue, C. H. Tan, G. F. Liu and Y. Y. Zhao, *Org. Biomol. Chem.*, 2005, **3**, 2508–2512.
6 C. Y. Bao, R. Lu, M. Jin, P. C. Xue, C. H. Tan, T. H. Xu, G. F. Liu and Y. Y. Zhao, *Chem. – Eur. J.*, 2006, **12**, 3287–3294.
7 S. S. Babu, V. K. Praveen and A. Ajayaghosh, *Chem. Rev.*, 2014, **114**, 1973–2129.
8 R. J. Kumar, J. M. MacDonald, T. B. Singh, L. J. Waddington and A. B. Holmes, *J. Am. Chem. Soc.*, 2011, **133**, 8564–8573.
9 C. Vijayakumar, V. K. Praveen and A. Ajayaghosh, *Adv. Mater.*, 2009, **21**, 2059–2063.
10 P. C. Xue, P. Chen, J. H. Jia, Q. X. Xu, J. B. Sun, B. Q. Yao, Z. Q. Zhang and R. Lu, *Chem. Commun.*, 2014, **50**, 2569–2571.
11 P. C. Xue, Q. X. Xu, P. Gong, C. Qian, A. M. Ren, Y. Zhang and R. Lu, *Chem. Commun.*, 2013, **49**, 5838–5840.
12 X. C. Yang, R. Lu, T. H. Xu, P. C. Xue, X. L. Liu and Y. Y. Zhao, *Chem. Commun.*, 2008, 453–455.

13 X. L. Liu, X. F. Zhang, R. Lu, P. C. Xue, D. F. Xu and H. P. Zhou, *J. Mater. Chem.*, 2011, **21**, 8756–8765.
14 X. L. Liu, D. F. Xu, R. Lu, B. Li, C. Qian, P. C. Xue, X. F. Zhang and H. P. Zhou, *Chem. – Eur. J.*, 2011, **17**, 1660–1669.
15 X. F. Zhang, X. L. Liu, R. Lu, H. J. Zhang and P. Gong, *J. Mater. Chem.*, 2012, **22**, 1167–1172.
16 X. C. Yang, R. Lu, F. Y. Gai, P. C. Xue and Y. Zhan, *Chem. Commun.*, 2010, **46**, 1088–1090.
17 S. Pradhan, S. Sagiri, V. Singh, K. Pal, S. Ray and D. Pradhan, *J. Appl. Polym. Sci.*, 2014, DOI: 10.1002/APP.39979.
18 P. C. Xue, R. Lu, Y. Huang, M. Jin, C. H. Tan, C. Y. Bao, Z. M. Wang and Y.-Y. Zhao, *Langmuir*, 2004, **20**, 6470–6475.
19 N. M. Sangeetha and U. Maitra, *Chem. Soc. Rev.*, 2005, **34**, 821–836.
20 J. W. Steed, *Chem. Commun.*, 2011, **47**, 1379–1383.
21 S. S. Babu, S. Prasanthkumar and A. Ajayaghosh, *Angew. Chem., Int. Ed.*, 2012, **51**, 1766–1776.
22 Y. Xu, P. C. Xue, D. F. Xu, X. F. Zhang, X. L. Liu, H. P. Zhou, J. H. Jia, X. C. Yang, F. Y. Wang and R. Lu, *Org. Biomol. Chem.*, 2010, **8**, 4289–4296.
23 B.-K. An, J. Gierschner and S.-Y. Park, *Acc. Chem. Res.*, 2012, **45**, 544–554.
24 S. J. George, A. Ajayaghosh, P. Jonkheijm, A. P. H. Schenning and E. W. Meijer, *Angew. Chem., Int. Ed.*, 2004, **43**, 3422–3425.
25 A. Ajayaghosh and S. J. George, *J. Am. Chem. Soc.*, 2001, **123**, 5148–5149.
26 J. J. V. Gorp, J. A. J. M. Vekemans and E. W. Meijer, *J. Am. Chem. Soc.*, 2002, **124**, 14759–14769.
27 S. S. Babu, K. Kartha and A. Ajayaghosh, *J. Phys. Chem. Lett.*, 2010, **1**, 3413–3424.
28 S. Wakim, J. Bouchard, M. Simard, N. Drolet, Y. Tao and M. Leclerc, *Chem. Mater.*, 2004, **16**, 4386–4388.
29 H. Ebata, T. Izawa, E. Miyazaki, K. Takimiya, M. Ikeda, H. Kuwabara and T. Yui, *J. Am. Chem. Soc.*, 2007, **129**, 15732–15733.
30 J. Yu, J. Luo, Q. Chen, K. He, F. Meng, X. Deng, Y. Wang, H. Tan, H. Jiang and W. Zhu, *Tetrahedron*, 2014, **70**, 1246–1251.
31 V. M. Svetlichnyi, E. L. Aleksandrova, L. A. Myagkova, N. V. Matyushina, T. N. Nekrasova, R. Y. Smyslov, A. R. Tameev, S. N. Stepanenko, A. V. Vannikov and V. V. Kudryavtsev, *Semiconductors*, 2011, **45**, 1339–1345.
32 Y.-L. Wu, Y.-N. Li, S. Gardner and B. S. Ong, *J. Am. Chem. Soc.*, 2005, **127**, 614–618.
33 V. M. Svetlichnyi, E. L. Alexandrova, L. A. Miagkova, N. V. Matushina, T. N. Nekrasova, A. R. Tameev, S. N. Stepanenko, A. V. Vannikov and V. V. Kudryavtsev, *Semiconductors*, 2010, **45**, 1581–1587.
34 J.-H. Tsai, C.-C. Chueh, M.-H. Lai, C.-F. Wang, W.-C. Chen, B.-T. Ko and C. Tin, *Macromol.*, 2009, **42**, 1897–1905.
35 S. Cai, G. Tian, X. Li, J. Su and H. Tian, *J. Mater. Chem. A*, 2013, **1**, 11295–11305.
36 T. Vehoff, B. Baumeier, A. Troisi and D. Andrienko, *J. Am. Chem. Soc.*, 2010, **132**, 11702–11708.
37 A. Kistenmacher and K. Müllen, *J. Heterocycl. Chem.*, 1992, **29**, 1237–1239.
38 D. Curiel, M. Más-Montoya, A. Uruvakili, R. A. Orenes, H. Pallamreddy and P. Molina, *Org. Lett.*, 2010, **12**, 3164–3167.
39 Y.-J. Cheng, C.-H. Chen, Y.-J. Ho, S.-W. Chang, H. A. Witek and C.-S. Hsu, *Org. Lett.*, 2011, **13**, 5484–5487.
40 M. Wang, Y. Li, H. Tong, Y. Cheng, L. Wang, X. Jing and F. Wang, *Org. Lett.*, 2011, **13**, 4378–4381.
41 D. Wasserfallen, M. Kastler, W. Pisula, W. A. Hofer, Y. Fogel, Z. Wang and K. Müllen, *J. Am. Chem. Soc.*, 2006, **128**, 1334–1339.
42 G. K. B. Clentsmitha, L. D. Fielda, B. A. Messerlea, A. Shashaa and P. Turnerb, *Tetrahedron Lett.*, 2009, **50**, 1469–1471.
43 F.-J. Zhang, C. Cortez and R. G. Harvey, *J. Org. Chem.*, 2000, **65**, 3952–3960.
44 X. F. Zhang, X. P. Qiu, R. Lu, H. P. Zhou, P. C. Xue and X. L. Liu, *Talanta*, 2010, **82**, 1943–1949.
45 T. Naddo, Y. Che, W. Zang, K. Balakrishnan, X. Yang, M. Yen, J. Zhao, J. S. Moore and L. Zhang, *J. Am. Chem. Soc.*, 2007, **129**, 6978–6979.
46 J. S. Yang and T. M. Swager, *J. Am. Chem. Soc.*, 1998, **120**, 11864–11873.

